Cluster evolution in a cold Ising ferromagnet: Disappearance of magic numbers with temperature rise

B. J. Kooi*

Department of Applied Physics, Zernike Institute for Advanced Materials and Netherlands Institute for Metals Research, University of Groningen, Nijenborgh 4, 9747 AG Groningen, The Netherlands

(Received 16 July 2007; revised manuscript received 22 October 2007; published 9 January 2008)

Decay and growth of clusters at low and intermediate temperatures based on the two-dimensional square-lattice Ising model has been studied with Monte Carlo simulations employing Glauber (or Metropolis) dynamics, exploiting a procedure where the starting configuration is a cluster (that tend to grow in the applied magnetic field) on a relatively small lattice. The behavior of such a cluster is stochastic and only when typical several thousands of identical clusters are analyzed will the underlying deterministic behavior become apparent. At $0.4T_c$, the time-dependent cluster size distribution is relatively broad, but smooth, i.e., Gaussian, and the decay and growth behaviors of various relative compact clusters are compared. At lower temperatures, modulations in the size distribution occur with minima at magic sizes corresponding to $n=m\times m+1$ and $n=m\times(m+1)+1$ with m integer values. A quantitative analysis of the amplitude of the modulations as a function of temperature is performed. Also the relation between the distributions of size and of the number of internal cluster bonds (or cluster perimeter) is scrutinized.

DOI: 10.1103/PhysRevB.77.024303 PACS number(s): 64.60.Q−, 05.50.+q, 02.70.Uu, 64.60.My

I. INTRODUCTION

Most phase transitions proceed via nucleation and growth, and such transitions occur in a wide variety of systems (from atomic to astronomic length scales) in nature and technology. For instance, nucleation plays a key role in most materials production, having an important influence on the final product performance. Understanding nucleation processes is, therefore, of great importance. Complex behavior emerging from systems based on relatively simple but (physically) interesting (first principles) rules may help in understanding nucleation.[1–7] In this light, the popularity of research on dynamic Ising models can be understood. Also, the present work is dedicated to this field of research by focusing on cluster evolution at relatively low temperatures within the two-dimensional (2D) square-lattice Ising model studied using Monte Carlo (MC) simulations.

MC simulations of low-temperature processes are generally inefficient, because the transition probabilities decrease exponentially with temperature when the common dynamics, e.g., of Glauber (or Metropolis) type, are used.[8–10] Excessive large number of MC steps and, for certain processes, large systems (e.g., spatial scales) have to be used for obtaining adequate results, or the dynamics has to be implemented in a more intelligent manner.[11,12] To avoid such problems, many kinetic studies involving MC simulations of the 2D square-lattice Ising model were performed at relatively high temperatures.[1,6,13–17] However, also MC simulations have in recent years been performed explicitly at low temperatures,[12,18,19] albeit for strong fields such that the critical cluster size remained extremely small. Still, for $T\rightarrow 0$, analytical (in conjunction with numerical) work on the 2D square-lattice Ising model dominates.[3,7,20–22] In deriving nucleation properties from MC simulations, particularly at low temperatures, it has been popular to determine metastable lifetimes.[6,12,14,18,19] However, then the information on the time-dependent distribution of cluster sizes and shapes intimately linked to nucleation remains generally unknown.

A major complexity of low temperatures and weak fields (small driving forces) is that the number of different cluster configurations involved in nucleation is huge.[17,23,24] In the isotropic case (holding, in general, at high temperatures), cluster properties are only a function of the number of monomers (spins, atoms, etc.) n they contain. Clusters decay or grow by stepwise release or attachment of a monomer ($n-1$ and $n+1$). Although a complete picture of (both steady state and transient) nucleation is far from trivial in this one-dimensional case,[2] the complexity strongly increases when clusters with the same n can have a large variety in shapes and energies, as is already the case within the relatively simple 2D square-lattice Ising model for $n\geqslant 6$.[17,22,23] For example, for $n=19$, 20, and 21, the total number of *distinct* cluster configurations on the 2D square lattice is over 5.9×10^9, 22×10^9, and 88×10^9, respectively.[17] In principle, all *possible* transitions with their energies and probabilities between all configurations for such $n-1\leftrightarrow n\leftrightarrow n+1$ have to be considered from $n=0$ to n clearly larger than the critical nucleus size n^* in order to arrive at a complete picture of nucleation. Fortunately, the situation improves at low temperatures, since cluster energy will prevail over entropy and, thus, for each n, only clusters with the lowest possible energies have to be considered. Then, most configurations can be discarded and the one-dimensional case is again approached. For instance, for $n=19$, 20, and 21, the number of clusters with the lowest energy (two lowest energies) is 8 (922), 2 (428), and 187 (7835), respectively.[17]

At such low temperatures, a cluster grows by keeping its shape most compact, i.e., with minimal perimeter. This implies square $m\times m$ and rectangular $m\times(m+1)$ shapes, i.e., with {10} facets. The critical nucleus, as derived by Neves and Schonmann for $T=0$, is then the $n^*=m^*\times(m^*+1)$ rectangle with an extra spin on the longer side, where m^* is defined by $m^*=\mathrm{floor}(2J/H)$ with $J(>0)$ the ferromagnetic coupling constant and H the external magnetic field used in

the standard Ising Hamiltonian [cf. Eq. (1) below].[3] The operation "floor" means rounding to the lower nearest integer number. Directly above $T=0$, also the intermediate $n=m^2+1$ clusters can become critical nuclei.[23] The higher the temperature (below T_c), the more these discrete values of n due to the specific low energy configurations become replaced by the continuous spectrum of all integer n values due to configurational entropy. In fact, at low temperatures, not only the critical nuclei have discrete "magic" sizes, but the whole semiequilibrium distribution (number densities) of noninteracting clusters will show strong modulation as a function of cluster size.

Recently, an impressive development has been presented (based on considerable cumulative work), providing analytical expressions for calculating the transient nucleation fluxes, taking into account thousands of different low energy cluster configurations.[7] Although still Metropolis dynamics was involved, the calculations did not rely on the traditional numerical Monte Carlo simulations, and thus could be applied well to low temperatures, as should be since only low energy configurations were considered. The most interesting result of applying the expressions to the 2D square-lattice Ising model at low temperatures was the observed collapse of fluxes around selected magic cluster sizes. In the light of the discussion given above, the occurrence of magic sizes is not so surprising, as can be expected for a system having a strong modulation in energy of clusters as a function of their size and, thus, in their semiequilibrium distribution. Nevertheless, the actual observation of simplifying patterns in the complexity of multidimensional nucleation paths is of great importance.

Although the present work is of simpler scope, it is also devoted to the occurrence of magic sizes during growth and decay of clusters in the 2D square-lattice dynamic Ising model. A comparison with analogous results for the 2D hexagonal dynamic Ising model will be presented in another paper. The main aim here is to quantitatively explain the disappearance of magic cluster sizes with increasing temperature. To this purpose, MC simulations have been performed at low and intermediate temperatures, i.e., for T_c/T in between 2.5 and 6 (and relatively weak fields $H<0.8$, typically around 0.4), using a procedure with artificial injection of clusters on relatively small lattices that has not been applied before to the 2D square-lattice Ising model.[25] This specific approach was chosen in order to still observe significant dynamic behavior with sufficient statistics when using MC simulations (with Metropolis or Glauber dynamics) at low temperatures within tractable temporal and spatial scales.

II. MODEL AND NUMERICAL METHODS

The model used is the standard 2D square-lattice Ising model defined by the Hamiltonian:

$$H = -J\sum_{\langle i,j\rangle} s_i s_j - H\sum_i s_i, \tag{1}$$

with a ferromagnetic coupling constant $J>0$ between the spins s having ± 1 value and with an external magnetic field H; $\langle i,j\rangle$ indicates summation over all nearest neighbor pairs. Of course, an equivalent lattice gas model could have been adopted as well. In order to study dynamic processes within the model, stochastic Glauber dynamics was considered, where the spin-flip probabilities are defined by[8]

$$P[s_i \to -s_i] = \frac{\exp(-\beta\Delta E)}{1+\exp(-\beta\Delta E)}, \tag{2}$$

with ΔE the energy change due to the spin flip and $\beta = 1/k_B T$, with k_B the Boltzmann constant and T the temperature. The energy change is defined by

$$\Delta E = 2s_i\left(J\sum_{nn} s_j + H\right), \tag{3}$$

with nn meaning the nearest neighbor sites of site i. In some explicit cases, also Metropolis dynamics was used, where the spin-flip probability is defined by[9]

$$P[s_i \to -s_i] = \min[1, \exp(-\beta\Delta E)], \tag{4}$$

where, of course, for T approaching zero, Glauber and Metropolis dynamics become equivalent. A convenient scheme is to scale J and k_B to unity, defining the temperature with respect to the critical temperature T_c given according to Onsager's exact solution:[26]

$$T_c = 2/\ln(\sqrt{2}+1).$$

A standard algorithm is used, in which sites on a defined lattice (having appropriate boundary conditions) are chosen at random and flipped according to the probabilities given by Eq. (2) or (4). The evolution of the spin configurations on the lattice is followed as a function of the number of Monte Carlo steps performed. Time is given in units of Monte Carlo steps per site (MCSS), i.e., in one unit, the number of MC steps performed is equal to the number of lattice sites.

A standard procedure would start with a lattice where all spins are metastably aligned in one direction, and then studying the development and evolution of clusters with spins aligned in the opposite stable direction for certain applied fields H and certain temperatures T. Similarly, a system can first be equilibrated in a certain field, after which the direction of the field is reversed and the evolution of spins and/or clusters can be followed. A different approach is adopted in the present work due to the specific low-temperature problems of MC simulations mentioned in the Introduction. This approach is partly based on a procedure mentioned and applied by Shneidman *et al.*[25] There, the starting configuration was a relatively small hexagonal (triangular) lattice with an artificially injected nucleus. The decay and/or growth of such nuclei with different initial radii R were studied in order to derive kinetic parameters. The spin-flip probabilities were defined by the so-called Jackson-Kilmer-Temkin model and were not small, i.e., not comparable with the Metropolis or Glauber dynamics at low temperatures. The work presented there gives the impression that individual nuclei, although showing some stochastic behavior, overall behave deterministically, satisfying decay and growth rates that are explicit functions of R. For the 2D square-lattice Ising model with Metropolis or Glauber

dynamics, individual nuclei behave completely stochastically. In order to obtain the underlying deterministic behavior, sufficient statistics is required, i.e., meaning, for the present work, that the evolution of typically several thousand initially identical nuclei has to be followed. In this sense, the present work clearly deviates from the approach in Ref. 25, but the procedure of nuclei artificially injected in relatively small lattices is reproduced here. Emphasis is on injection of clusters with compact shape, since these are the clusters naturally occurring at low temperatures.

An important question is if it is justified to study the evolution of individual isolated clusters and neglect potential coalescence with neighboring clusters. The answer to this question for the present work is yes, since the sizes of the clusters currently considered are, in all cases, sufficiently smaller than the ones holding when coalescence (fusion) of the clusters would occur. Clusters are still within the nucleation regime, where they can grow but also can decay, and are definitely not in a supercritical regime governed by cluster-cluster interactions. Proof for this is provided in the Appendix. The standard lattice contained 32×32 sites, but the results presented here, as tested, remained identical for increased lattice sizes of 64×64 and 128×128 sites, and probably larger lattices. Only when the time scales used in the MC simulations are much longer than considered in the present work and when the lattice sizes are larger (than 128×128) does the single-droplet regime go over in the multiple-droplet regime.

An important aspect of the simulations is the evolution of cluster size and cluster perimeter (or number of internal bonds in a cluster) as a function of time. These were evaluated using the efficient Hoshen-Kopelman (HK) algorithm,[27] which was originally developed for percolation studies. For the present study where on a (small) lattice a single cluster was artificially injected, only the evolution of this single cluster was of interest. This could be conveniently followed, at the low temperatures considered, by always taking the size of the largest cluster (with its perimeter and number of internal bonds) found on the lattice by the HK algorithm. The cluster size n is defined as the total number of connected spins with one orientation (i.e., which have at least one neighbor with the same orientation), where a cluster is surrounded by spins of opposite orientation.

Energies E_n^b of clusters on the 2D square lattice are defined by their size n and their perimeter length L_n^b or the number of internal (nearest neighbor) bonds b present within the cluster, because $L_n^b=4n-2b$ (Refs. 22 and 23):

$$E_n^b = 2(JL_n^b - nH), \tag{5a}$$

$$E_n^b = 4J\left[2n\left(1-\frac{H}{4J}\right)-b\right]. \tag{5b}$$

Based on these energies, the semiequilibrium distribution (number density) D_n^b of noninteracting clusters can be derived:[23]

$$D_n^b = w_n^b \exp(-\beta E_n^b), \tag{6}$$

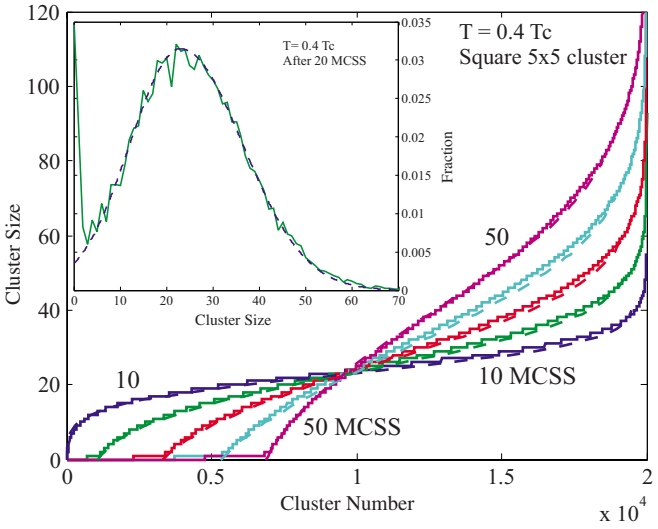

FIG. 1. (Color online) Results of Monte Carlo simulations (solid lines) showing the cluster-size distributions after various times (in MCSS ranging from 10 to 50 in steps of 10) based on the evolution of 20 000 clusters, all initially square 5×5, at a temperature of $T=0.4T_c$ in a magnetic field $H=0.36$. Fits to the solid lines based on symmetric Gaussian distributions are given by dashed lines. The inset shows the cluster-size distribution after 20 MCSS based on the MC simulations as a solid line and a fit based on an asymmetric Gaussian distribution as a dashed line.

where w_n^b is the total number of configurations possible for given n and b. For the 2D square lattice, the w_n^b values were obtained recently up to $n=17$ (Refs. 23 and 24) and up to $n=21$.[17] Due to the relatively low temperatures and fields H used in the present work, also larger clusters will be studied for which the w_n^b values are still unknown.

III. RESULTS AND DISCUSSION

A. $T=0.4T_c$

The evolution of cluster size as a function of time (in MCSS) is shown in Fig. 1 for $T=0.4T_c$, $H=0.36$, and 20 000 clusters having an initial shape and size of square 5×5 (i.e., with {10} facets). The cluster sizes during the evolution at each time can be described well on the basis of a Gaussian distribution, when excluding the clusters with $n<3$. Symmetric Gaussian distributions are represented by dashed curves in Fig. 1 and can reproduce adequately the solid curves based on MC simulations. The inset in Fig. 1 shows, instead of the cumulative distribution, the usual size distribution, i.e., cluster fraction versus cluster size after 20 MCSS including an asymmetric Gaussian fit. Of course, allowing some asymmetry in the width of the Gaussian distribution improves the fitting, which now is nearly perfect.

All curves tend to pivot around a central point from which the final fraction of clusters that will decay and vanish (and the complementary fraction of clusters that are able to grow) can be extrapolated. After 50 MCSS, nearly 25% of the clusters decayed to a size zero, but the pivot point indicates that the final fraction will be about 49%–50%. A kinetic definition of the critical nucleus would imply one having an equal

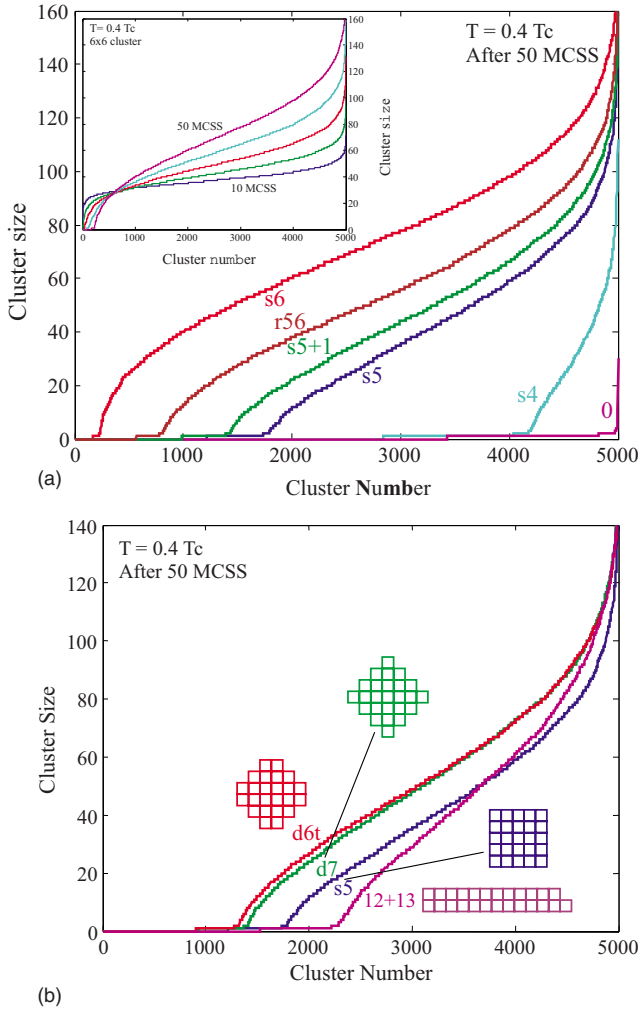

FIG. 2. (Color online) Cluster-size distributions obtained by MC simulations after a time of 50 MCSS at $T=0.4T_c$ and $H=0.36$ for various initial cluster sizes and shapes. (a) 5000 initially identical clusters with the following size and shapes were used for the simulations: square clusters with 16, 25, and 36 spins; rectangular 5×6 clusters; and square 5×5 clusters having one spin added to the middle of a side. Also, the 0 distribution is shown, meaning that initial clusters were not present in this case. The inset shows the size distribution for the square 6×6 cluster after various times (in MCSS ranging from 10 to 50 in steps of 10). (b) 5000 initially identical clusters, with the various sizes and shapes as explicitly indicated, were used for the simulations.

chance to grow or decay after long times.[16,23] In this sense, the 5×5 square cluster can be called critical, since adding or removing one pixel from the 25 moves the decay and growth fractions away from 50%. For instance, compare in Fig. 2(a) the curves denoted s(quare)5 and s5+1, where one spin is added to the (noncorner) side of the s5 cluster. The temperature $T=0.4T_c$ is clearly too high for having critical clusters defined by the Neves-Schonmann criterion or the intermediate m^2+1 clusters. Possibly $n=25$ fits within the phase diagrams of Figs. 2 and 3 shown in Ref. 23. However, these diagrams go up to a maximum value $n=17$ and, instead of a kinetic definition, are based on thermodynamic criteria. A unique definition of a critical cluster size does not exist. As is

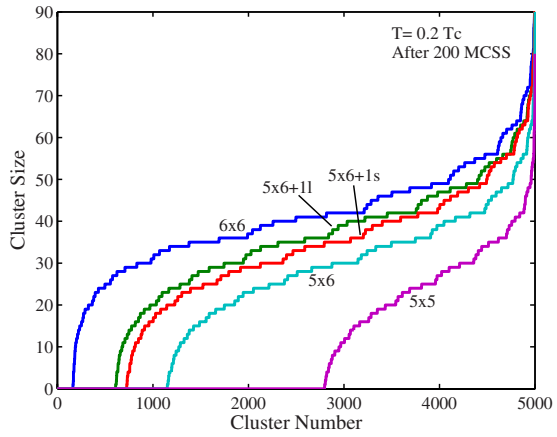

FIG. 3. (Color online) Results of MC simulations showing for various initial cluster sizes and shapes the cluster-size distributions after a time of 200 MCSS at $T=0.2T_c$ and $H=0.36$. 5000 initially identical clusters with the following size and shapes were used for the simulations: square clusters with 25 and 36 spins, rectangular 5×6 clusters, 5×6 clusters with a spin added to (a noncorner site on) the short side, and 5×6 clusters with a spin added to (a noncorner site on) the long side. Instead of the smooth distributions occurring at $0.4T_c$ (cf. Figs. 1 and 2), now clear variations in step lengths can be observed.

shown in Fig. 2(b) per type of shape, a critical cluster size can be defined, but different types can have different critical cluster sizes. In particular, for nucleation rates, the probability (number density) that certain shapes develop is important. In this sense, exotic shapes may have a small critical size based on a kinetic definition, but if the probability that they develop is minimal, their influence on the overall nucleation rate will also be little.

The pivot point present in Fig. 1 is universally observed. All curves rotate best around the pivot if the initial cluster is close to the critical size, showing 50% decay and growth as in Fig. 1. However, also when the initial cluster clearly deviates from the critical one, a pivot can be clearly recognized on the scale shown in Fig. 1 and is then useful to estimate the critical size and the final fraction growth (or decay) after long times [see inset in Fig. 2(a)]. Apparently, already early during the dynamic process, the fractions that decay and grow become fixed, giving rise to the pivot point.

The distribution of cluster sizes after 50 MCSS at $0.4T_c$ is shown in Fig. 2 for different initial cluster shapes and sizes. Figure 2(a) shows that the square 6×6 and 4×4 clusters (s6 and s4, respectively) are clearly beyond and below the critical size, with extrapolated decay fractions of 11% and 89%, respectively. The curve indicated as 0 shows that with 5000 "empty" initial areas (32×32 spins) only in one did a cluster grow beyond the critical size, and more than 99% of the areas contained a largest cluster with $n<3$. This explains why the Gaussian distributions in Fig. 1 did not apply to clusters with $n<3$; these clusters lost correlation with the initially injected clusters and showed correlation with the empty (initial) area. The 0 curve demonstrates that already at $T=0.4T_c$ useful MC simulations of nucleation and growth without the use of injected clusters would require large spatial and temporal scales.

Excluding the d6t curve, the other three curves in Fig. 2(b) hold for $n=25$ clusters. The diamond shaped d7 cluster having {11} facets [see inset in Fig. 2(b) for its detailed shape] shows significantly less decay than the s5 cluster. This can be readily understood since growth of the d7 ($n=25$) to the s7 ($n=49$) is possible by addition of spins that have two nearest neighbors aligned parallel ("double-bonded" spins), whereas growth of the s5 cluster to s7 requires two additions of a "single-bonded" spin (adatom on a smooth facet), corresponding to a strongly activated step having a low probability. One could now tend to conclude that clusters with {11} facets have the highest growth probability. This conclusion is not justified as is demonstrated in Fig. 2(b) by the curve of the d6t cluster with $n=24$ (see inset for its shape) showing a larger growth fraction than the d7 one with $n=25$. Also here *a posteriori* reasoning is possible. The d7 cluster contains four single-bonded spins that have large probability to disappear first. Therefore, direct growth with only double-bonded spins of the d7 to the s7 cluster as mentioned above is unlikely; it may as well transform into the s5 state. On the other hand, such single-bonded spins are absent in the d6t cluster. This cluster is, thus, less vulnerable to decay and is likely to grow with only double-bonded spins to the s6 cluster.

Up to now, all curves for a certain time did not show any crossings. However, this is possible as demonstrated in Fig. 2(b) by the curves pertaining to s5 and the 12+13 clusters. This last elongated cluster type (only two units thick) is more vulnerable to decay than the s5 cluster (i.e., exhibits larger decay fraction), but, nevertheless, shows after 50 MCSS a larger fraction of large clusters with $n>52$. Compared to s5, the width of the Gaussian distribution for the 12+13 cluster increases faster in time, indicating both faster growth and decay kinetics.

B. $T=0.2T_c$

When reducing the temperature from $0.4T_c$ to $0.2T_c$ (keeping $H=0.36$), interesting changes are invoked. The critical nucleus increases from, say, the 5×5 to the 5×6 cluster with one spin added. The distribution of cluster sizes after 200 MCSS at $0.2T_c$ is shown in Fig. 3 for different initial cluster sizes. The 5×6, the $5\times6+1$s, i.e., one spin added to a noncorner site on the short side, and the $5\times6+1$l, i.e., one spin added to a noncorner site on the long side, exhibit an extrapolated growth fraction of 40%, 55%, and 63%, respectively. So, the addition of one spin on the side of a rectangular cluster causes a large increase in growth probability at this low temperature, whereas the effect is limited to only a few percent at $0.4T_c$. From these three cluster types, the one with one spin added to the short side is closest to the kinetic definition of a critical nucleus. Increasing H to 0.37 gives the 5×6 cluster nearly exact 50% growth and 50% decay probabilities. These results show that, according to the kinetic definition, already at low temperatures the critical cluster size exhibits a continuous spectrum of all integer numbers and not only magic numbers like m^2+m+1 or m^2+1 as found according to the thermodynamic definition(s) of Ref. 23. Changing from Glauber to Metropolis dynamics does not result in important differences.

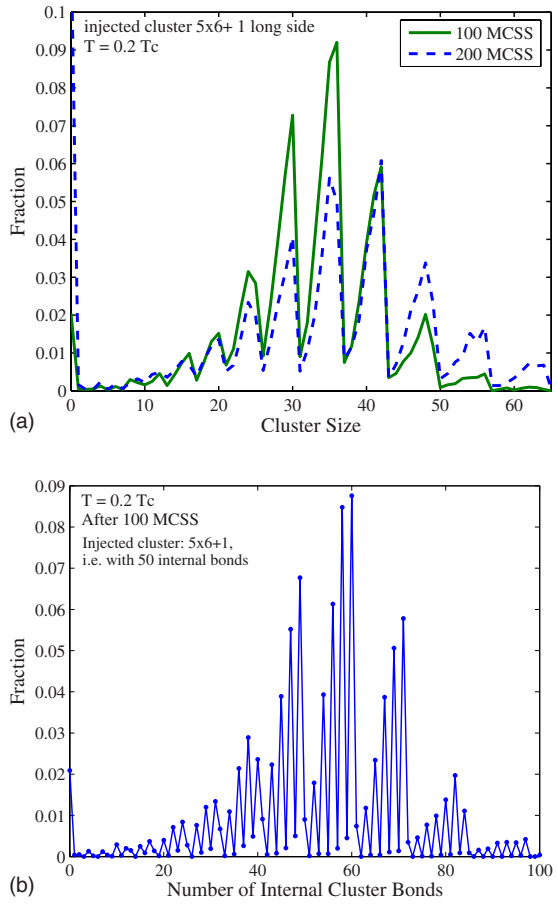

FIG. 4. (Color online) MC simulation results holding for $T=0.2T_c$ and $H=0.36$ for 10 000 initially injected 5×6 clusters with a spin added to (a noncorner site on) the long side. (a) Cluster-size distribution after 100 and 200 MCSS. Strong modulation in the cluster-size distributions are present with minima at $n=m\times m+1$ and $n=m\times(m+1)+1$. (b) Distribution of the number of internal cluster bonds after 100 MCSS showing that on top of the modulations that can be attributed to the size effect, a higher frequency modulation (with generally a period of 2) is present, showing that for each size the lowest-energy configuration strongly dominates.

At $0.2T_c$, now 80% of the 5×5 clusters decay, whereas this fraction was 50% at $0.4T_c$. For the 6×6 cluster, also a clear difference exists: 24% decay at $0.2T_c$ versus 11% decay at $0.4T_c$. With increasing temperature (and relatively weak field $H<1$), the activated step needed for growth (addition of a single-bonded spin) has a probability that increases more strongly than the probability of erosion of corner sites. Therefore, growth becomes more dominant at higher temperatures and the critical cluster size decreases.

Instead of smooth curves as for $0.4T_c$, now curves with large nonuniformity in step length occur. Instead of the cumulative distribution as presented in Fig. 3, the standard size distribution for the $5\times6+11$ clusters is shown in Fig. 4(a) for 100 and 200 MCSS. The smooth Gaussian distributions at $0.4T_c$ have now obtained at $0.2T_c$ a strong modulation on top. Analysis of the modulation shows that minima always occur for $n=m\times m+1$ and $n=m\times(m+1)+1$. The values of these minima can be readily understood, since compact m

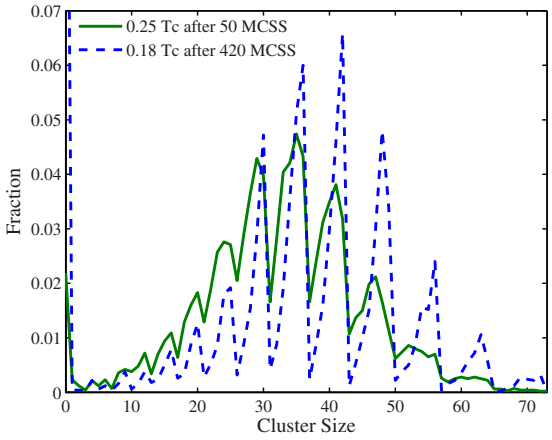

FIG. 5. (Color online) Cluster-size distribution for 10 000 initial 5×6 clusters with a spin added to (a noncorner site on) the long side holding for a magnetic field $H=0.36$ and after times that have been scaled (see text for details) to allow a direct comparison of the two temperatures $0.18T_c$ and $0.25T_c$. The modulations in the size distribution become weaker, and the peak shape changes from sawtooth to more symmetric when the temperature is increased. Although the decay and growth processes are strongly activated by temperature, the scaling indicates that the processes occur less efficiently at higher temperatures, because also higher energy paths are followed.

$\times m$ and $m\times(m+1)$ shapes with one spin added to a side are very unstable (high energy, short living) configurations which easily decay to $m\times m$ and $m\times(m+1)$, but also can grow quickly to $m\times(m+1)$ and $(m+1)\times(m+1)$ or $m\times(m+2)$. This also directly relates to the observed collapse of fluxes around the ones pertaining to the magic cluster sizes.[7]

The maxima show more intriguing behavior. For instance, after 200 MCSS, maxima at $n=m\times m$ are absent, but occur at $m\times(m+1)$ and $m\times(m+2)$ [and $m\times(m+3)$]. When explicitly considering the fractions for $n=35$ and $n=36$, one can see that the initial higher fraction for 36 is taken over by 35. The equilibrium number densities of the 6×6 and 5×7 clusters [based on Eqs. (5) and (6)] would give a ratio $\exp(-22.08/T)/2\exp(-22.8/T)=2.44$. However, removing one of the four corners of the 6×6 cluster gives identical cluster size and energy as the 5×7 cluster and, hence, a more correct ratio is $\exp(-22.08/T)/6\exp(-22.8/T)=0.81$. So, there is a configurational (entropic) reason that the fraction of m^2-1 increases, in general, with respect to the one for m^2. This becomes more apparent in Fig. 5. However, the above calculation is simplified; for instance, the large number of next lowest-energy configurations for $n=36$ are also relevant. Taking them into account, the 36 peak should remain larger than the 35 peak. So, another reason should exist that makes the occurrence of m^2-1 clusters more likely than m^2 ones. The reason has interesting kinetic origin, because the $(m-1)\times(m+1)$ clusters have difficulty to grow, i.e., they have only one-sided connection with the lowest-energy path and are, thus, in a "metastable trap,"[7] and will thus be longer living "droplets" than the $m\times m$ or $m\times(m+1)$ clusters. This is also exactly the reason why the 5×6 cluster with one spin added to the short side shows more decay and less growth in Fig. 3 than when the extra spin is added to the long side.

Instead of the distribution of the cluster sizes n, also that of the number of internal cluster bonds b can be shown; this is done in Fig. 4(b) for the 100 MCSS curve presented in Fig. 4(a). The sawtooth modulation observed in Fig. 4(a) can be traced back in Fig. 4(b), but on top, an even stronger modulation with a shorter period of generally 2 can be found; i.e., a strong variation in the fractions (number densities) for b and $b+1$. From this variation, it can be concluded that for each n, the cluster-size distribution at $0.2T_c$ is (already) strongly dominated by the lowest-energy configuration.

C. Magic sizes versus temperature

An intriguing issue is how, as a function of temperature, the size distribution evolves from smooth at relatively higher temperature ($0.4T_c$) to strongly peaked at lower temperature ($0.2T_c$). Size distributions for $0.18T_c$ and $0.25T_c$ are presented in Fig. 5 based on injected $5\times6+11$ clusters. As will be explained in the next paragraph, the times were scaled in order to obtain comparable results for different temperatures. Compared to $0.2T_c$, the distribution at $0.18T_c$ shows even more pronounced sawtooth behavior that can be related directly to the lowest possible energies of clusters "having an overall classical (Gibbs) outlook plus sharp sawtooth modulation."[7,22] At $0.25T_c$, the minima remain at identical position (m^2+1 and m^2+m+1), but the maxima shift such that the sawtooth is replaced by more symmetric peaks. Most importantly, the contrast between minima and maxima decreases for increasing temperature and, thus, vanishes approximately at $T=0.4T_c$ (see the inset in Fig. 1).

At low temperatures, growth occurs via compact shapes. The rate-determining step for growth is the addition of the first extra spin (adatom) to the side of a square or rectangular cluster. The probability p_{-2} of this activated step is directly obtainable from Eq. (2) or (4), giving approximately the same result for lower temperatures (for relatively weak fields H):

$$p_{-2}=\exp(-\beta[4J-2H]) \tag{7a}$$

and time can be scaled according to $\tau=1/p_{-2}$. This scaling was also applied in Ref. 7. Note that H is taken positive and that clusters are composed of positive spins in a surrounding of negative spins. However, when this first spin is added, it has a large probability to be removed in the next (MCSS) time periods. Only when it is stabilized by a second neighboring positive spin, transition from one compact shape to the next is likely. Therefore, for a compact cluster having a perimeter length L, a better approximation of the time scale for its transition to the next compact shape is

$$\tau=\left\{\left[(8)^{\frac{1}{2}}+(L-8)^{\frac{2}{3}}\right]p_{-2}p_0\right\}^{-1}\quad(L\geqslant 8), \tag{7b}$$

where p_0 is given by

$$p_0=\exp(2\beta H)/[1+\exp(2\beta H)]. \tag{7c}$$

In Fig. 5, time scaling (with p_{-2} as dominant term) was applied to make the comparison between the results of $0.18T_c$ and $0.25T_c$. It is interesting that after scaling, growth

at lower temperatures proceeds relatively faster. This can be deduced from Fig. 5, but is a general feature observed for many more temperatures and initial clusters. Apparently, the scaling factor causes an overestimation that was already slightly reduced by the introduction of the p_0 factor. The reason for this overestimation is that at lower temperatures, growth proceeds via lower energy paths than at higher temperatures, i.e., occurs clearly more selective and efficient. At higher temperatures, growth also occurs via less favorable cluster configuration for further growth (e.g., metastable traps). This is not accounted for in the scaling factor since it assumes that growth proceeds via the same path(s) with the same rate-limiting step(s).

Quantification of the evolution of the contrast C between the maxima and minima as a function of temperature was done as follows. 5×6 or $5\times6+11$ clusters were injected and followed during their dynamic evolution. Based on these results, the ratio of the peak fraction for $n=30$, F_{30}, and the cusp fraction for $n=31$, F_{31}, is obtained as a function of time, i.e., $C=F_{30}/F_{31}$. Injection of $5\times6+11$ clusters quickly results in a stable value for this ratio (the contrast C). The 5×6 clusters are used to see if they converge to the same contrast value, but this occurs much slower. For instance, at $0.2T_c$, the $5\times6+11$ clusters converge to a stable contrast value within 20 MCSS, whereas for the 5×6 clusters, a similar value is approached after 200 MCSS. In this way, reliable converged values for the contrast C were obtained for various temperatures. Apart from Glauber dynamics, also for various temperatures, Metropolis dynamics was used to obtain C. No significant differences were found, although decay and growth dynamics itself occurs generally faster when using Metropolis (where the difference vanishes when approaching zero temperature). In Fig. 6, $\ln(C)$ is plotted versus T_c/T using data points. One can see that below $0.4T_c$, the contrast slowly increases, but below $0.22T_c$, $\ln(C)$ is nearly a linear function of T_c/T.

It would be interesting to model and understand the results in Fig. 6. The ratio of the 30 peak with respect to the 31 cusp was chosen because it has minimum kinetic influence. The 30 peak has no problems with a (nearby) metastable trap like that present for the 35-36 region. Moreover, the Gaussian distribution on top of which the strong contrast modulation occurs is for the magnetic field used, generally peaked near $n=31$. The contrast C would be kinetically affected if the peak and cusp would be positioned on the flank of the Gaussian distribution. Now the C values in Fig. 6 should have dominant thermodynamic origin, i.e., based on the semiequilibrium distribution [Eq. (6)]:

$$C=\frac{F_{30}}{F_{31}}\approx\sum_{b\,\min}^{b\,\max}D_{30}^{b}\Bigg/\sum_{b\,\min}^{b\,\max}D_{31}^{b}=\sum_{b\,\min}^{b\,\max}w_{30}^{b}\times\exp(-\beta E_{30}^{b})\Bigg/\sum_{b\,\min}^{b\,\max}w_{31}^{b}\exp(-\beta E_{31}^{b}). \quad (8)$$

However, it is currently not possible to obtain the w_{30}^{b} and w_{31}^{b} values from literature.[17,23,24] Instead, a first naive picture for C is that it is based on one 5×6 cluster versus 22 possibilities (perimeter length of the 5×6 cluster) to add a single spin to the sides of the 5×6 cluster. The result is given by the dashed straight (red) line in Fig. 6, and obviously does not match the "experimental" data. Nevertheless, it explains the observed slope of the experimental data at low temperatures. This leads to the conclusion that below $0.22T_c$, only the lowest-energy configurations for $n=30$ and $n=31$ dominate; the occurrence of other higher energy configurations is negligible. This is in agreement with the results presented in Fig. 4(b).

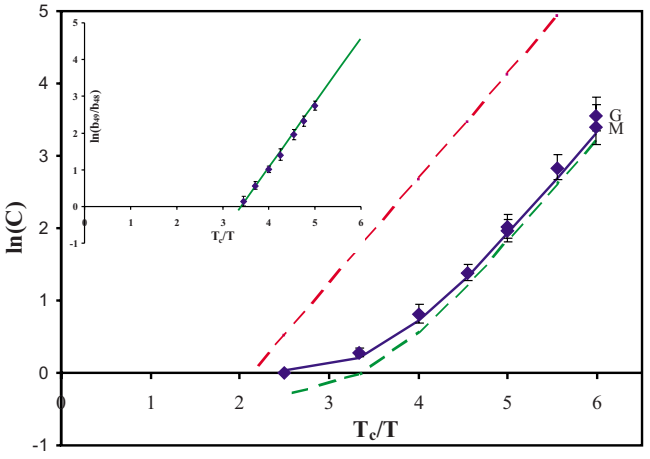

FIG. 6. (Color online) Ratio of the number density of clusters with a size $n=30$ and $n=31$, called contrast C, as a function of the reciprocal temperature T_c/T. The data points are results of MC simulations and the lines are based on theory, where the number density can be described by $D_n^b=w_n^b\exp(-E_n^b/k_BT)$, with E_n^b the energy of a cluster with size n and number of internal bonds b, k_B the Boltzmann constant, and w_n^b the number of distinct configurations for given n and b. The inset shows the ratio of 49 and 48 internal cluster bonds in the cluster with a size $n=30$ as obtained with the MC simulations and based on the same theoretical result from which the solid curve in the main graph was obtained. The excellent agreement between theory and MC simulations shows that, under kinetic conditions, local equilibrium conditions hold to a great extent.

In order to shift the theoretical prediction on the data, other configurations for the same cluster energy has to be introduced. The $n=31$ clusters are not only 5×6 clusters with one spin added to their sides, but identical energy holds if one of the corner spins of the cluster is removed and (instead of the single spin) one spin pair is added to the sides (4×16 possibilities). Similarly, two spins can be removed from the corners (either a pair from one corner or two singles from two corners) and one row of three spins (triplet) is added to the sides ($8\times11+6\times10$ possibilities—nine configurations that are now produced for the second time). Similarly, the second lowest-energy configuration of $n=30$ clusters can be introduced by removing one, two, or three spins from the corners and adding a single spin, a spin pair, or a spin triplet to the sides [4×20, $(8\times15+6\times14)$, $(12\times10+24\times9+4\times8-60)$ possibilities, respectively]. The result obtained in this way is the dashed (green) curve in Fig. 6. It is already close to the experimental data and shows reasonable curvature. If the next configurations with rows of four or five spins are added to the sides with additional removal of

the correct number of spins from the corners to obtain $n=30$ or $n=31$, the dashed curve first moves to the right away from the data. Only after finally obtaining the compact 6×5 cluster out of the initial 5×6 cluster does the prediction jump back to the left and the solid (blue) curve is obtained. This curve explains the observations very well.

A check of internal consistency can be performed based on the predictions for the probabilities that each of the two lowest-energy configurations occur for $n=30$. The most compact shape for $n=30$, i.e., the 5×6 and 6×5 clusters contain 49 internal bonds. Removing 1–5 spins from the corners and adding the same number in a single row to the side of these compact clusters yield the second most compact cluster with 48 internal bonds. The ratio of the number of clusters with 49 and 48 bonds versus the reciprocal temperature is shown in the inset of Fig. 6 both based on the MC simulations (data points) and theoretically based on Eq. (6) (straight line). The agreement is again excellent, showing that under dynamic kinetic conditions, locally thermodynamic equilibrium can prevail. Of course, equilibrium in the local size distribution cannot be present exactly, since, otherwise, further decay and growth would not occur at all.

What can we learn from the above results? For $0.4T_c>T>0.2T_c$, for each n, only the configurations with the two lowest energies are relevant to explain the contrast. These two energies are definitely necessary for the clusters with magic numbers (m^2 and m^2+m), where the next higher energy configurations occur by erosion of corner sites (removal of double-bonded spins), which is compensated by an additional row of spins on a side. For the cluster configurations corresponding to the cusps, the second lowest-energy configurations are clearly less important. Note that when the contrast vanishes, the relative error due to considering only lowest-energy contributions strongly increases, but the absolute error remains small.

Below $0.2T_c$, for each n, only the lowest energy configuration is relevant. For the clusters with magic numbers (m^2 and m^2+m), erosion of corner sites is possible, but these states are so short living that they have negligible influence on the number density of states with magic numbers. Interestingly, the conclusions drawn in the present and previous points do not depend on the magnetic field H, but depend on the cluster size. This is an exact result, because it can be derived directly from Eqs. (5) and (6) that the dependence on H disappears when comparing the relative importance of the configurations with different energies (i.e., with a difference in number of bonds p) for a certain n:

$$\frac{D_n^{b-p}}{D_n^b}=\frac{w_n^{b-p}\exp(-\beta E_n^{b-p})}{w_n^b\exp(-\beta E_n^b)}=\frac{w_n^{b-p}}{w_n^b}\exp(-\beta 4Jp). \quad (9)$$

The dependence on cluster size can also be understood via Eq. (9), because the ratio of the number of configurations with the lowest (having number of bonds $b_{\max}$) and second lowest energy (having one bond less) $w_n^{b_{\max}-1}/w_n^{b_{\max}}$ is increasing with increasing cluster size[17,23] and, therefore, the temperature below which only the lowest-energy configuration is relevant decreases with increasing cluster size.

Growth occurs for $T<0.4T_c$ via a layer by layer, i.e., step-flow mechanism. The probability that on a second {10} facet of a compact cluster a single spin (adatom) is formed (i.e., with only one neighboring spin aligned parallel) before another layer has completely closed (either by decay or growth) is negligible. Erosion occurs by removal of corner sites (spins having two neighbors aligned parallel). The final result is, of course, the interplay of simultaneously occurring growth and erosion, leading to the stochastic behavior with broad size distributions.

D. Simulation of cluster size and bond distributions

The contrast C, shown in Fig. 6, holds for a particular field H and for a particular pair of cluster sizes ($n=30$ and 31). Larger fields H or larger sizes of the cluster pair [$n=Y$ and $Y+1$, where Y is $m\times m$ or $m\times(m+1)$] leads to a decrease of the contrast C at a certain (low) temperature. It is clear that in the limit of large Y, the contrast C has to disappear.

Instead of calculating the contrast on the basis of only a single cluster pair, it would be interesting to see if the whole size distribution can be simulated at low temperatures. At $0.4T_c$, the size distribution could be described well by a (symmetric) Gaussian one. Based on this result, one can consider that actually the semiequilibrium distribution (number density) has to be multiplied with a Gaussian distribution. However, then it is needed that the (whole) semiequilibrium distribution is quantifiable. At present, this is only possible for $n\leqslant21$, since only for these n values the w_n^b values required in Eq. (6) were obtained[17] by using the remarkably smart and short algorithm of Redner.[28] To apply Redner's algorithm up to $n=25$ is currently practically impossible.[17,23,24] Therefore, at the moment, it is appropriate to consider the size distributions for $n\leqslant21$. To take a part of the above distributions, where the maximum of the Gaussian distribution and the injected cluster size occur at clearly higher values than $n=21$, is not useful. Therefore, results were generated where the field H was increased from 0.36 to 0.45 and the injected cluster was reduced in size to $4\times4+1$. The cluster-size distribution as obtained from the corresponding MC simulations are shown in Fig. 7(a) for $T=0.2T_c$ after 50 MCSS and for $T=0.3T_c$ after 25 MCSS. An attempt was made to reproduce these MC results by using the semiequilibrium distribution as calculated from Eqs. (6) and (5), where for each n only the two lowest-energy configurations were included. The deviation in the results when including the third lowest-energy configuration is not more than a few percent for only the compact cluster shapes at $0.3T_c$, whereas in all other cases the deviation is clearly less. The equilibrium distribution contains no free (adjustable) parameters. In order to reproduce the MC simulation, the equilibrium distribution was multiplied by a Gaussian distribution containing three adjustable parameters, i.e., the position and height of the maximum and the width of the distribution. The result is shown in Fig. 7(b) again for $0.2T_c$ and $0.3T_c$. In quantitative sense, some clear deviations are present between the MC calculations in Fig. 7(a) and the size distribution simulation in Fig. 7(b), particularly at $0.3T_c$, but in a more

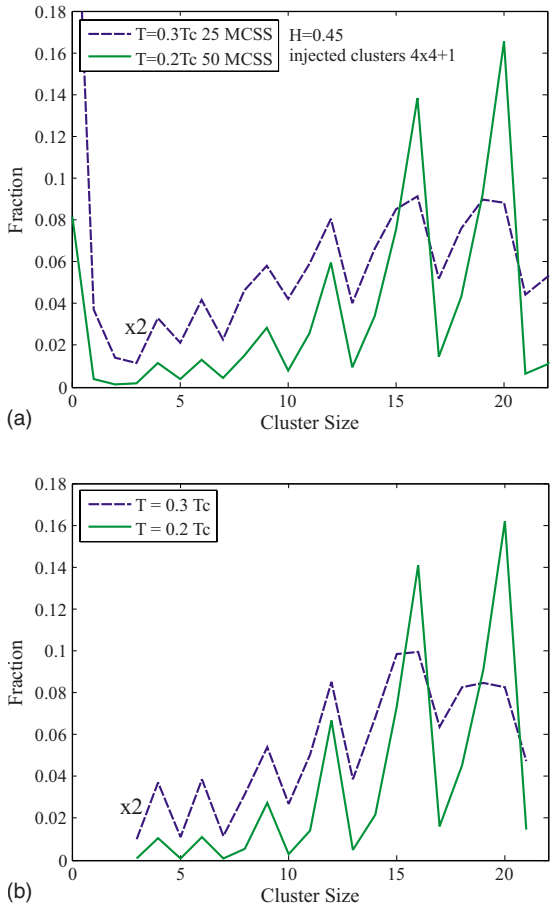

FIG. 7. (Color online) (a) Cluster-size distributions obtained with MC simulations for 10 000 initial 4×4 clusters with a spin added to a noncorner site in a magnetic field $H=0.45$ at $T=0.2T_c$ after 50 MCSS and at $T=0.3T_c$ after 25 MCSS. (b) Cluster-size distributions obtained in order to reproduce the results in (a) by multiplying the known semiequilibrium distribution based on the two lowest-energy configurations at each size n ($\leqslant 21$) with a symmetric Gaussian distribution having three adjustable parameters (position, height, and width).

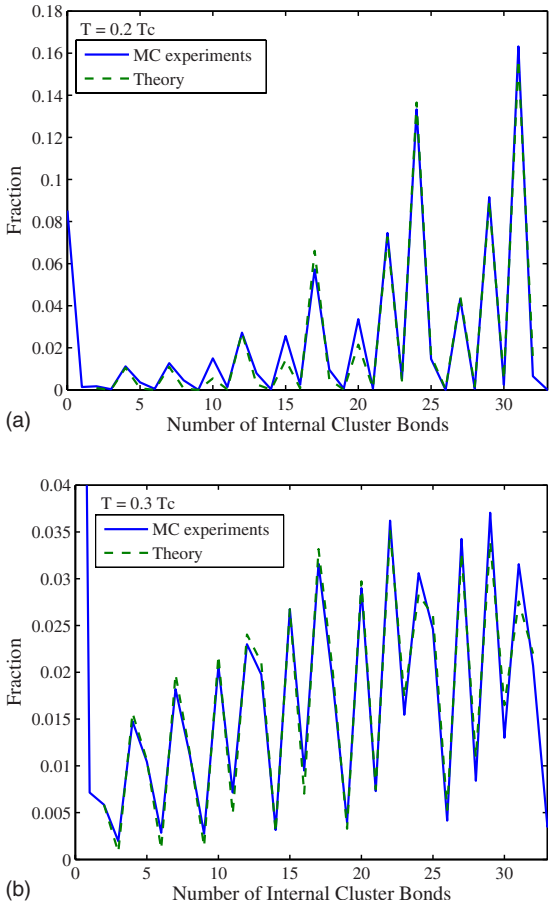

FIG. 8. (Color online) Distribution of the number of internal cluster bonds based on MC simulations (solid line) and based on theory (dashed line), which was also used to reproduce the results of Fig. 7(a) in Fig. 7(b). Note that in the transition from Fig. 7(b) to Fig. 8, only the lowest-energy configuration for each number of internal cluster bond is taken into account and that there are no adjustable parameters. (a) MC results hold for $H=0.45$ at $T=0.2T_c$ after 50 MCSS. (b) MC results hold for $H=0.45$ at $T=0.3T_c$ after 25 MCSS.

general and qualitative sense the agreement is remarkably good. For instance, the reduction in contrast when going from $0.2T_c$ to $0.3T_c$, corresponding to the reduction in height of the maxima and simultaneous increase in the minima, is well captured in the simulations. Moreover, also the change from clear sawtooths at $0.2T_c$ to broader, more symmetric peaks as observed at $0.3T_c$ in Fig. 7(a) and similarly observed in Fig. 5 is also reproduced in Fig. 7(b). In particular, the relative fractions at $n=15$ and 16 when going from $0.2T_c$ to $0.3T_c$, where m^2-1 increases strongly with respect to m^2, is nicely reproduced. See also the similar discussion with respect to the observed relative fractions for $n=35$ and 36 at the end of Sec. III B.

The distribution of the number of internal cluster bonds b, D_b, can now be calculated directly from the known size n distribution, D_n, without the use of any adjustable parameter. This is definitely not trivial as also shown by the cluster enumeration literature (or literature on counting lattice animals), where only in recent work the number of configuration with a given size and given number of internal bonds was calculated.[17,23] Earlier, the total number of configurations for a given size was determined without subdivision into different numbers of internal bonds for the same size. Calculating D_b from D_n was done using the following assumptions: (i) for each b value, only the lowest-energy configuration is taken into account, meaning that for most n values, the two lowest-energy configurations are included [only at the minima in the size n distribution, i.e., at $n=m\times m+1$ and $n=m\times(m+1)+1$, not two but one lowest-energy configuration is included], and (ii), that for each n, the division over these two b values is determined by Eq. (6). If this procedure is applied to the theoretically calculated size n distribution of Fig. 7(b) holding for $0.2T_c$, the dashed curve in Fig. 8(a) is obtained. When it is compared with the results directly provided by the MC simulations (solid line), the agreement is in most instances excellent. The dominant deviations are already caused by the differences in the size n distribution present between Figs. 7(a) and 7(b), because if

the same procedure is applied to the size n distribution directly obtained from the MC simulations and compared with the distribution of the number of internal cluster bonds obtained from the MC simulations, no visual difference between the two curves can be observed. If this last procedure is applied at $0.3T_c$, the results in Fig. 8(b) are produced. In this case, the deviations between the experimental and theoretical curves become visible, but are still small, indicating that taking only the lowest-energy configuration associated with each b value into account still produces adequate results at this temperature. The results at $0.2T_c$ [Fig. 8(a)] show that the second lowest-energy configuration for a given n produces states in the b distribution in Fig. 8(a) very close to zero, implying that at $0.2T_c$, only the lowest-energy configuration for each n is important. At $0.3T_c$ definitely the two lowest-energy configurations for each n are relevant. Moreover, the comparison between MC simulations and the theory shows that, for the dynamic conditions used, the thermodynamic Eqs. (5) and (6) are appropriate to calculate how the total number of states at each n is distributed over the different b configurations having this n.

IV. CONCLUSIONS

The growth and decay of clusters at low and intermediate temperatures within the two-dimensional square-lattice Ising model (in various magnetic fields H) were studied using Monte Carlo simulations employing Glauber (or Metropolis) dynamics, exploiting a procedure with "injection" of a cluster on a relatively small lattice. The behavior of individual clusters is stochastic and only when typical several thousands of identical clusters are injected does their underlying deterministic evolution become apparent.

At $0.4T_c$ (or higher temperature), initially identical clusters show after a certain time a relatively broad Gaussian size distribution. Below $0.4T_c$, modulations in the size distribution appear, with minima at magic sizes corresponding to $n=m\times m+1$ and $n=m\times(m+1)+1$, with m integer values. At sufficiently low temperature, typically $\leqslant 0.2T_c$, maxima occur at sizes corresponding to $n=m\times m$ and $n=m\times(m+1)$, and the modulations have clear sawtooth shape. Increasing the temperature from $0.2T_c$ to $0.4T_c$, the sawtooth shape is gradually replaced by more symmetric peaks and the depressions at the minima gradually vanish.

This temperature-dependent behavior could be reproduced well on the basis of the semiequilibrium distribution (number density) of noninteracting cluster [cf. Eq. (6)]. Unfortunately, this equilibrium distribution is only known for cluster sizes up to 21, recently obtained using Redner's algorithm. However, for larger clusters, still calculations can be made because of the simplifying fact shown by the present MC simulations that below $0.4T_c$, only the two lowest-energy configurations for each cluster size have to be taken into account and, below $0.2T_c$, only the lowest-energy configuration (a result that is independent of magnetic field H, but dependent on cluster size n; for larger clusters, these transition temperatures go down). In this way, the relative presence of clusters with $n=30$ and $n=31$ could be calculated, showing excellent agreement with the results of MC simulations.

The results show that, under kinetic conditions, locally in the size distribution the equilibrium distribution can be used; the kinetic size distribution can be reproduced by multiplying the equilibrium distribution with a Gaussian distribution. If the size distribution is known, also the perimeter-length distribution or the distribution for the number of internal cluster bonds can be calculated directly via Eqs. (5) and (6).

APPENDIX

Analysis of the growth of individual isolated clusters, as performed in the present work, is only justified if they remain smaller than the size at which, under normal conditions, they would meet and coalesce with neighboring clusters. Therefore, it is important to derive the length scale associated with coalescence D_0 and compare it with the one holding for a critical nucleus D_C. Using droplet theory and Monte Carlo simulations, extensive analysis of the various length scales involved in the two-dimensional square-lattice Ising model has been performed at $0.8T_c$.[14,15] At this temperature, it was shown (Fig. 11) in Ref. 15 that for magnetic fields $H\leqslant 0.8(J)$, D_C always remained (typically a factor 5) smaller than D_0.[29] At temperatures lower than $0.8T_c$, the difference between D_0 and D_C is expected to increase. To show explicitly that this expectation is correct, the analysis given below is performed.

For a constant nucleation rate I and a constant growth velocity v in d-dimensional space, the following relation can be derived for D_0 (Refs. 14 and 15):

$$D_0 = A\left(\frac{v}{I}\right)^{1/(d+1)}. \tag{A1}$$

Depending on the specific (growth) conditions, A can vary, but its value will be near 1 and $A=1$ is adopted here, like in Ref. 14. A constant nucleation rate pertains to the kinetic Ising model,[14,15] but the growth velocity increases with cluster size, where a maximum constant growth velocity v_0 occurs for a (infinitely long) planar interface. An explicit formulation of v_0 for the 2D square-lattice Ising model with Glauber dynamics and an interface that is parallel to one of the symmetry directions of the lattice is given by[15,30]

$$v_0(T,H) = \frac{\tanh(\beta H)}{(1+X)^2}\left\{2X + \frac{1+X^2}{1+Y^2} + \frac{X^2}{1-X^2} \times\left[X^2 + \frac{2(1+2X)}{1+Y^2}\right]\right\}, \tag{A2}$$

where $X=\exp(-2\beta J)\cosh(\beta H)$ and $Y=\sinh(2\beta J)/\cosh(\beta H)$ (other symbols have been defined in Sec. II). In Eq. (A1), $v=v_0/2$ will be used.

Since nucleation in the Ising model in the present context is governed by discrete microscopic effects, we cannot rely on a continuum meso- or macroscopic theory like droplet theory to estimate I for a large range of temperatures (and fields). Instead, we use an upper bound for the nucleation rate, derived in Ref. 23, that employs information from the semiequilibrium distribution on the 2D square lattice [Eqs. (5) and (6) in Sec. II]:

$$I \ll (2n^* + 2)\exp(-\beta\langle W\rangle_{n^*}), \tag{A3a}$$

where

$$\langle W\rangle_{n^*} = 8Jn^*\left(1 - \frac{H}{4J}\right) - \beta^{-1}\ln\left(\sum_{b=b_{\min}(n^*)}^{b_{\max}(n^*)} w_{n^*}^{b}\exp(4\beta Jb)\right). \tag{A3b}$$

Since we use an upper bound for I, the coalescence length scale D_0 calculated with Eq. (A1) will be a lower bound, since I will still compensate the effect of a potentially too high value for the velocity v. Results of the calculation are shown in Fig. 9. First, a value for the magnetic field H was chosen. At low temperatures, H determines n^* over a large temperature range.[23] Then, for such a H, n^* pair, Eqs. (A1)–(A3) allow calculation of D_0 as a function of temperature. For $n^*=7$, 13, and 21, the summation in Eq. (A3) contains 3, 7, and 13 terms, respectively.

The results in Fig. 9 show that below about $0.5T_c$, the lower bound of D_0 is already larger than D_C. Note that at these low temperatures clusters tend to have compact shapes such that the $n^*=7$, 13, and 21 clusters will fit in 3×3, 4×4, and 5×5 areas and, thus, D_C can be taken as 3, 4, and 5, respectively. At higher temperatures, less compact, more elongated shapes come into play and D_C due to anisotropy is less well defined, but, of course, cannot exceed n^*, the length of a linear chain. Figure 9 also indicates that below $0.5T_c$, the ratio D_0/D_C increases for decreasing fields H.

At temperatures higher than $0.5T_c$, the present results indicate that D_0 is smaller than D_C. This is probably not actually true since the obtained D_0 is a lower bound. Also, the use of the fixed H, n^* pairs is, in principle, not correct at higher temperatures (for a certain H, n^* decreases with increasing temperature[23]), gives some underestimation of D_0, but the effect is calculated to be minor. The fact that the present D_0 calculations give a lower bound is in agreement with the results at $0.8T_c$ presented in Ref. 15, where D_0 is still larger than D_C. The purpose of the present appendix is to demonstrate that at the relatively low temperatures used for the calculations in the main text ($T\leqslant0.4T_c$ and for not too high fields, i.e., $H<1$, in the 2D square-lattice Ising model), it is correct to consider individual isolated clusters with sizes around the critical ones. Indeed, already the conservative estimation presented here proves this to be correct.

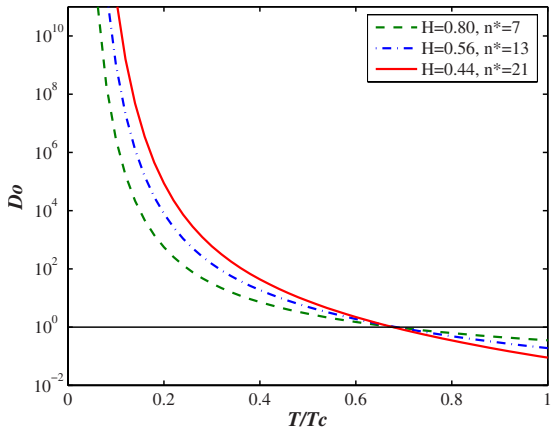

FIG. 9. (Color online) Length scale D_0, giving a lower bound for the size that the clusters can grow before they meet and coalesce with neighboring clusters, versus the relative temperature T/T_c for three different values for the magnetic field H. The results clearly indicate that below $0.5T_c$, the critical cluster size is smaller than D_0. The analysis of the evolution of individual isolated clusters, as performed in the present work, is thus justified.

*b.j.kooi@rug.nl

[1] M. E. Fisher, Physics (Long Island City, N.Y.) **3**, 255 (1967).
[2] K. F. Kelton, A. L. Greer, and C. V. Thompson, J. Chem. Phys. **79**, 6261 (1983).
[3] E. J. Neves and R. H. Schonmann, Commun. Math. Phys. **137**, 209 (1991).
[4] P. A. Rikvold and B. M. Gorman, in *Annual Reviews of Computational Physics I*, edited by D. Stauffer (World Scientific, Singapore, 1994), p. 149.
[5] S. Auer and D. Frenkel, Nature (London) **409**, 1020 (2001).
[6] K. Brendel, G. T. Barkema, and H. van Beijeren, Phys. Rev. E **71**, 031601 (2005).
[7] V. A. Shneidman and G. M. Nita, Phys. Rev. Lett. **97**, 065703 (2006).
[8] R. J. Glauber, J. Math. Phys. **4**, 294 (1963).
[9] N. Metropolis, A. W. Rosenbluth, M. N. Rosenbluth, A. H. Teller, and E. Teller, J. Chem. Phys. **21**, 1087 (1953).
[10] H. Müller-Krumbhaar and K. Binder, J. Stat. Phys. **8**, 1 (1973).
[11] M. A. Novotny, in *Annual Reviews of Computational Physics IX*, edited by D. Stauffer (World Scientific, Singapore, 2001), p. 153.
[12] M. A. Novotny, Comput. Phys. Commun. **147**, 659 (2002).
[13] D. Stauffer and J. Kertesz, Physica A **177**, 381 (1991).
[14] P. A. Rikvold, H. Tomita, S. Miyashita, and S. W. Sides, Phys. Rev. E **49**, 5080 (1994).
[15] R. A. Ramos, P. A. Rikvold, and M. A. Novotny, Phys. Rev. B **59**, 9053 (1999).
[16] V. A. Shneidman, K. A. Jackson, and K. M. Beatty, Phys. Rev. B **59**, 3579 (1999).
[17] S. Frank, D. E. Roberts, and P. A. Rikvold, J. Chem. Phys. **122**, 064705 (2005).
[18] K. Park, P. A. Rikvold, G. M. Buendia, and M. A. Novotny, Phys. Rev. Lett. **92**, 015701 (2004).
[19] G. M. Buendia, P. A. Rikvold, K. Park, and M. A. Novotny, J. Chem. Phys. **121**, 4193 (2004).
[20] A. Bovier and F. Manzo, J. Stat. Phys. **107**, 757 (2002).
[21] V. A. Shneidman and G. M. Nita, Phys. Rev. Lett. **89**, 025701 (2002).
[22] V. A. Shneidman, J. Stat. Phys. **112**, 293 (2003).

[23] V. A. Shneidman and G. M. Nita, J. Chem. Phys. **121**, 11232 (2004).
[24] G. M. Nita, J. Comput. Phys. **206**, 578 (2005).
[25] V. A. Shneidman, K. A. Jackson, and K. M. Beatty, J. Chem. Phys. **111**, 6932 (1999).
[26] L. Onsager, Phys. Rev. **65**, 117 (1944).
[27] J. Hoshen and R. Kopelman, Phys. Rev. B **14**, 3438 (1976).
[28] S. Redner, J. Stat. Phys. **29**, 309 (1982).
[29] A requirement of droplet theory is that the critical cluster diameter $D_C \gg 1$, corresponding at $0.8T_c$ to $H \ll 0.78$ (J). This requirement is not really satisfied in Ref. 15.
[30] P. A. Rikvold and M. Kolesik, J. Stat. Phys. **100**, 377 (2000).